




Redox imbalance induces remodeling of glucose metabolism in *Rhipicephalus microplus* embryonic cell line

Received for publication, October 5, 2021, and in revised form, January 10, 2022. Published, Papers in Press, January 19, 2022.
<https://doi.org/10.1016/j.jbc.2022.101599>

Bárbara Della Noce^{1,2,‡}, Renato Martins da Silva^{1,2,‡}, Marcelle Vianna de Carvalho Uhl^{1,2}, Satoru Konnai³, Kazuhiko Ohashi³, Christiano Calixto^{1,2}, Angélica Arcanjo^{1,2}, Leonardo Araujo de Abreu^{1,2}, Stephanie Serafim de Carvalho^{1,2}, Itabajara da Silva Vaz Jr,^{2,4} and Carlos Logullo^{1,2,*}

From the ¹Laboratório de Bioquímica de Artrópodes Hematófagos, IBqM-UFRJ, Rio de Janeiro and Laboratório Integrado de Bioquímica Hatisaburo Masuda, NUPEM-UFRJ, Macaé, Rio de Janeiro, Brazil; ²Instituto Nacional de Ciência e Tecnologia em Entomologia Molecular, IBqM-UFRJ, Rio de Janeiro, Rio de Janeiro, Brazil; ³Laboratory of Infectious Diseases, Hokkaido University, Sapporo, Japan; ⁴Centro de Biotecnologia and Faculdade de Veterinária – UFRGS, Porto Alegre, Rio Grande do Sul, Brazil

Edited by Qi Qun Tang

Carbohydrate metabolism not only functions in supplying cellular energy but also has an important role in maintaining physiological homeostasis and in preventing oxidative damage caused by reactive oxygen species. Previously, we showed that arthropod embryonic cell lines have high tolerance to H₂O₂ exposure. Here, we describe that *Rhipicephalus microplus* tick embryonic cell line (BME26) employs an adaptive glucose metabolism mechanism that confers tolerance to hydrogen peroxide at concentrations too high for other organisms. This adaptive mechanism sustained by glucose metabolism remodeling promotes cell survival and redox balance in BME26 cell line after millimolar H₂O₂ exposure. The present work shows that this tick cell line could tolerate high H₂O₂ concentrations by initiating a carbohydrate-related adaptive response. We demonstrate that gluconeogenesis was induced as a compensation strategy that involved, among other molecules, the metabolic enzymes NADP-ICDH, G6PDH, and PEPCK. We also found that this phenomenon was coupled to glycogen accumulation and glucose uptake, supporting the pentose phosphate pathway to sustain NADPH production and leading to cell survival and proliferation. Our findings suggest that the described response is not atypical, being also observed in cancer cells, which highlights the importance of this model to all proliferative cells. We propose that these results will be useful in generating basic biological information to support the development of new strategies for disease treatment and parasite control.

Embryogenesis has been typically described as an energy-consuming process (1, 2). In the context of arthropods, the egg constitutes a closed system that relies solely on yolk contents for embryo energy supply and organ development (3–5). Therefore, once laid, the egg receives no nutrients from the external environment. An important model to study embryogenesis is *Drosophila melanogaster*, which also has

contributed to the understanding of cancer, neurological disorders, cardiovascular diseases, and several other human diseases. Genetic conservation between flies and humans is substantial, with 75% of known human disease genes having related sequences in *Drosophila* (6). Even under physiological conditions, fundamental metabolic processes, including energy metabolism, are well conserved among *Drosophila* and other animals (6). Consequently, hypotheses generated using this model are often relevant to many different areas of biological sciences. In cancer studies, *Drosophila* has served as a platform to develop models that recapitulate various aspects of the disease and its use has contributed to reveal different aspects of human malignant tumors (7, 8).

Research in *Drosophila* has served to determine how components of the insulin/insulin-like growth factor (IGF) system, including Rheb, Tsc1, and Tsc2, are organized in the insulin/Akt pathway and has contributed to define how insulin/Akt controls systemic and cellular growth (9–11). Those studies have expanded our knowledge of normal physiological roles these oncogenes and tumor suppressors play, as well as how their dysregulation promotes disease (12–14). Previous work by our group investigated the insulin-signaling pathway (ISP) and its possible role during tick embryogenesis, a controlled process of cell proliferation and differentiation, showing that those mechanisms are conserved in phylogenetically distant organisms, like insects, ticks, and mammals (15, 16). Also, determining if these aspects related to carbohydrate metabolism are relevant in the context of tumorigenesis and cancer metabolism is of great importance to support new cancer therapies.

A common feature of cancer cell metabolism is the ability to acquire necessary nutrients from a frequently nutrient-poor environment and utilize these nutrients to both maintain viability and build new biomass. Alterations in intracellular and extracellular metabolites that can accompany cancer-associated metabolic reprogramming have profound effects on gene expression, cellular differentiation, and tumor microenvironment (17). The major use of reduced carbon in proliferating cells is for the biosynthesis of a diverse array of

[‡] These authors contributed equally to this work.

* For correspondence: Carlos Logullo, carlos.logullo@bioqmed.ufrj.br.

Redox imbalance remodels the tick glucose metabolism

biomolecules, among which are fatty acids and cholesterol, pentose and hexose sugar derivatives, glycerol, nucleotides, and nonessential amino acids. This realization has spurred further exploration of advantages that the uncoupling of glycolysis from oxidative phosphorylation might offer to a proliferating cell. Although glycolysis is classically depicted as a single chain of molecular events that leads to the generation of pyruvate, a number of glycolytic intermediates can be diverted into branching pathways, generating diverse biosynthetic precursors (17). The preferential conversion of glucose into lactate, an altered metabolic feature typical of cancer cells known as the Warburg effect, has also been demonstrated in genetically normal proliferating cells, as well as in cells infected by viruses (18–20). These observations suggest that, rather than being an adaptation to defective respiration, the Warburg effect is a regulated metabolic state and may in fact be beneficial under a situation of increased biosynthetic demand (17).

Interest in cancer metabolism has grown rapidly in recent years, with an emphasis on understanding how cancer metabolism is reprogrammed and regulated, its influence on disease progression, and how these factors could be exploited to improve cancer therapy (21–23). In particular, genetic alterations that target PI-3 kinase, its negative regulators PTEN and INPP4B, as well as activating mutations and gene amplifications in a variety of upstream tyrosine kinase receptors, result in constitutive glucose uptake and metabolism in diverse cancer types (7, 24, 25). Being a point of convergence of signals from tyrosine kinase receptors as well as from the extracellular matrix, PI3K/Akt signaling represents a master regulator of glucose uptake. Metabolic reprogramming can induce oxidative stress tolerance and tumor progression in cancer cells (26, 27). Curiously, arthropod cells show a plasticity that supports higher tolerance to reactive oxygen species (ROS) when compared with mammalian cells, remarkably similar to the tolerance observed in cancer cells (28).

Aided by biochemical and molecular biology tools, arthropods are emerging as valuable models for studying cancer metabolism, to expand the current understanding of the mechanisms and functional consequences of tumor-associated metabolic alterations (7, 17). Therefore, arthropods have contributed to the study of mechanistic relationships between metabolism and cancer. Metabolic changes are increasingly recognized as important drivers of malignancy, and cancer-specific metabolic alterations are becoming an important research theme. Arthropods have been broadly used to study how metabolism is orchestrated to support biological processes, including growth, proliferation, and differentiation in normal development (5, 23, 29–31). The fact that these organisms share a gene conservation with humans and use similar metabolic reprogramming strategies can make them a valuable tool for comparative analysis with cancer metabolism. In addition, some arthropods have other experimental advantages, including a short life cycle and the ease with which large numbers of individuals can be examined in well-targeted genetic screens. In this context, the tick embryonic cell line, BME26 (31, 32), showed tolerance and resistance to oxidative stress similar to many different types of cancer cells, and the

present study explores its potential as a useful model of glucose metabolism in comparative and cancer research.

Results

Warburg effect and glycogen accumulation in response to oxidative challenge in arthropod embryonic cells

The effect of oxidative conditions on cell survival was compared among tick and other animal cells, including insect and mammals, to begin investigating the metabolic mechanisms related to H₂O₂ tolerance in BME26 tick embryonic cells after exposure to H₂O₂ (33). In general, with concentrations ranging from 62.5 to 1000 μM H₂O₂, arthropod embryonic cells (BME26 from *Rhipicephalus microplus*, Aag2 from *Aedes aegypti*, and S2 from *D. melanogaster*) were more tolerant than mammalian cells (primary culture of mouse macrophages and LLCMK2 kidney epithelial cells from *Rhesus monkey*) (Fig. 1A). The cell viability assay showed that S2 cells can tolerate up to 1 mM H₂O₂. Both mammalian cell lines presented H₂O₂-induced cytotoxic effects leading to reduced cellular viability; LD₅₀ values ranged between 125 to 250 μM H₂O₂ after 24 h of treatment (Fig. 1, A and B), in agreement with previous findings (30). In contrast, the mosquito embryonic cell line Aag2 exhibited cell proliferation at concentrations ranging from 125 to 250 μM H₂O₂, with up to 30% increase in viable cell numbers. Only at the highest tested concentration (1000 μM), H₂O₂ reduced by 20% the number of viable Aag2 cells (Fig. 1A). BME26 cells were unaffected by H₂O₂ at concentrations from 62.5 to 2000 μM.

The Warburg effect is well characterized in normal as well as highly proliferative cells, with high glucose uptake and conversion to lactate. We next analyzed glycogen and lactate levels in BME26 cells exposed to 2 or 4 mM H₂O₂ during 2, 6, 12, or 24 h. The analysis showed that BME26 cells accumulate glycogen up to 6 h after H₂O₂ addition, maintaining high glycogen levels until 24 h, in both H₂O₂ concentrations (Fig. 1C). After 48 h, the glycogen content returned to the same level observed in the control group (Fig. S1). Lactate levels increased in BME26 cells under 4 mM H₂O₂ at 2 and 6 h and under 2 mM at 12 h (Fig. 1C). The Aag2 insect cell line also showed an increase in glycogen level after 6 and 12 h of exposure to 2 mM H₂O₂ (Fig. S2).

ROS trigger increased glycogen levels in BME26 embryonic cells

To analyze glycogen metabolism in BME26 cells after H₂O₂ challenge, we analyzed the transcription of selected glycogen metabolism genes. Figure 2, A–D shows the transcriptional profile of glycogen synthase (GS), glycogen synthase kinase 3 β (GSK3β), phosphoglucomutase, and glycogen debranching enzyme (GDE) after exposure to 2 or 4 mM H₂O₂ for 2 h and 24 h. GS, the enzyme responsible for glycogen synthesis, showed increased transcription after 2 h at both H₂O₂ concentrations, being highest at 2 mM (Fig. 2A). GSK3β, the enzyme that inhibits GS activity, presented a transcriptional profile similar to that of GS, except after 2 h at 4 mM, when GSK3β transcription was similar to the control (Fig. 2B).

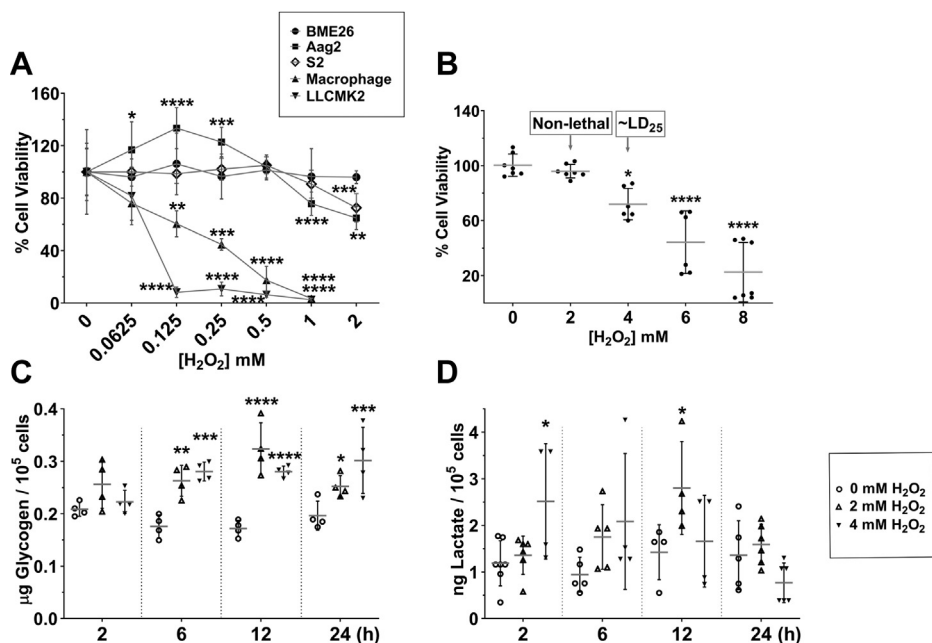


Figure 1. The Warburg effect and glycogen accumulation in response to oxidative challenge in arthropod embryonic cells. *A*, cell viability (trypan blue exclusion) was compared after challenge with H_2O_2 (62.5–1000 μM), in five different cell lineages, for 24 h: embryonic *Rhipicephalus microplus* tick cells (BME26), closed circles; embryonic *Aedes aegypti* cells (Aag2), closed squares; embryonic *Drosophila melanogaster* cells (S2), open diamond; BLACK6 mouse macrophage cells (primary culture), triangle up; renal epithelial *Rhesus monkey* cells (LLCMK2), triangle down. Control culture was performed at 0 μM H_2O_2 (100% of cells). *B*, BME26 cell viability upon H_2O_2 challenge (0–8 mM). Glycogen and lactate quantification over time (2, 6, 12, and 24 h) after H_2O_2 challenge in BME26 (*C* and *D*, respectively). Experiments were performed in three independent biological samples with three experimental replicates each, where $*p < 0.05$, $**p < 0.01$, $***p < 0.001$, $****p < 0.0001$, compared with the control, in Tukey's multiple comparisons test.

Phosphoglucomutase is an enzyme present in both glycogen synthesis (glucose 6-phosphate [G6P] to glucose 1-phosphate) and degradation (glucose 1-phosphate to G6P) pathways. Its transcription in BME26 cells after oxidative challenge followed

a profile similar to that of GSK3 β (Fig. 2C). In turn, GDE transfers three of the four glucose residues to other glycogen branches after the glycogen phosphorylase step. Its transcription in BME26 cells 2 h after oxidative challenge remained

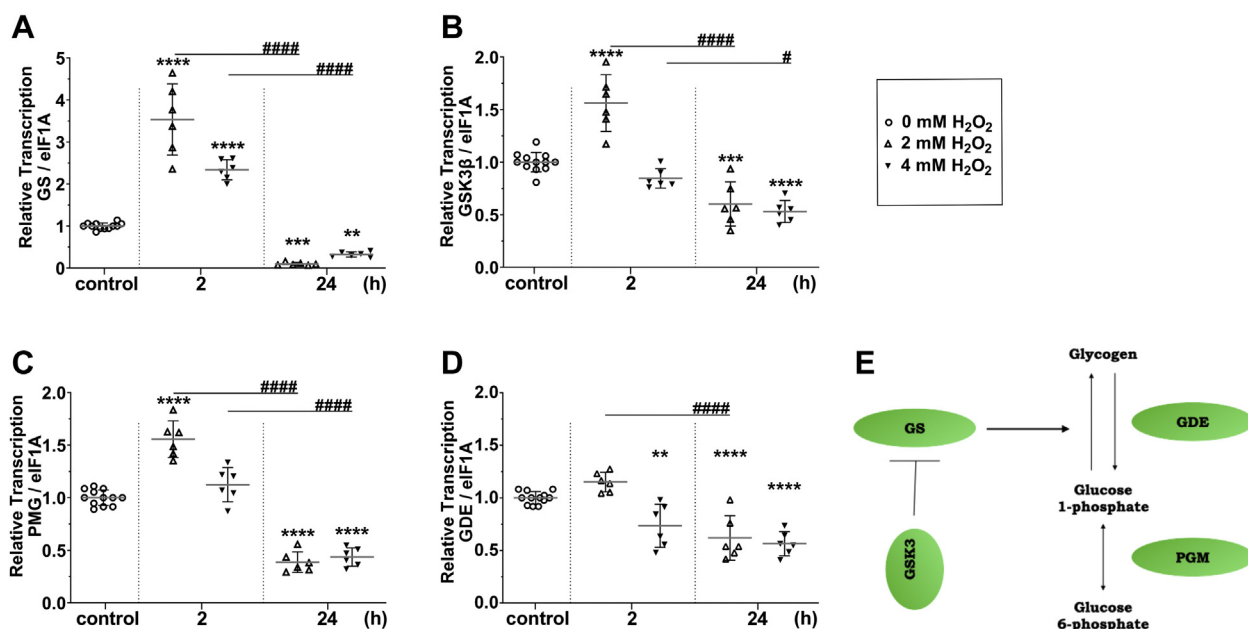


Figure 2. Oxidative challenge upregulates transcriptional levels of glycogen synthesis components in BME26 cells. Transcription of (*A*) glycogen synthase (GS), (*B*) glycogen synthase kinase 3 β (GSK3 β), (*C*) phosphoglucomutase (PGM), and (*D*) glycogen debranching enzyme (GDE) in *Rhipicephalus microplus* embryonic cell line (BME26) was measured 2 and 24 h after addition of H_2O_2 (2 or 4 mM). *E*, diagram of glycogen metabolism depicting pathways involved in glycogen synthesis and degradation. Experiments were performed in three independent biological samples with three experimental replicates each, where $**p < 0.01$, $***p < 0.001$, $****p < 0.0001$, compared with the control; and $\#p < 0.05$, $####p < 0.0001$, compared between the groups, in Tukey's multiple comparisons test.

Redox imbalance remodels the tick glucose metabolism

equal to the control condition, with a reduction in mRNA levels 24 h after H₂O₂ exposure (Fig. 2D). Thus, the transcription of genes related to glycogen metabolism in BME26 cells is shown to be regulated by oxidative conditions.

To further understand glycogen metabolism in BME26 cells treated with hydrogen peroxide, GS immunolocalization was performed, using antibodies that allow the detection of both total GS content and its inhibited (Ser641 phosphorylated) form. Cells were also treated with DAPI to stain the nuclei for imaging (Fig. 3A).

Images show that, under both H₂O₂ conditions, there was an increase in total as well as phosphorylated GS, colocalized with DAPI-stained cell nuclei (Fig. 3, B–D), in 2 h. The phosphorylated form, even with low catalytic activity, is still regulated by intracellular levels of G6P, its allosteric activator. After 24 h, the cellular distribution of the two forms of GS (active and inactive) is equivalent between the treated cells and the control condition (Fig. 3A, bottom).

The amount of GS protein also increased 2 h after H₂O₂ challenge, the phosphorylated form. When phosphorylated, GS is less active compared with the nonphosphorylated form. However, the phosphorylated form is also regulated allosterically by the amount of G6P, which leads to glycogen synthesis, a possible cause for the glycogen accumulation observed 6 h after H₂O₂ challenge (Fig. 1C). In addition, glycogen staining by Periodic acid–Schiff was performed to identify glycogen compartmentalization (Fig. 3E). We were able to see strong perinuclear staining (red arrows) after H₂O₂ challenge compared with a more diffuse marking in the untreated control (blue arrows). Differences are most evident 24 h after oxidative challenge is applied to BME26 cells. A representative scheme of the regulation of GS is described in Fig. 3F.

Gluconeogenesis–insulin pathways contribute to glycogen accumulation

To investigate carbohydrate metabolism, particularly concerning glycogen, glucose internalization was measured, showing that the staining of 2NBDG, a glucose analogue, increased after H₂O₂ exposure (Fig. 4, A and B). Decrease in 2NBDG staining was observed only 24 h after exposure to 4 mM H₂O₂ (Fig. 4, A and B). The exposed cells were also allowed to grow in two different media, namely, low or normal glucose concentration, and a cell viability assay was performed. A decrease in cell viability was observed at the highest H₂O₂ challenge condition, 4 mM. However, under low-glucose conditions, this reduction in viability was more pronounced compared with the normal glucose condition (Fig. 4C). The activity of regulatory enzymes of the glycolytic pathway also changed after the administration of H₂O₂. Hexokinase (HK) activity increased 2 h after H₂O₂ challenge and decreased to levels similar to the control condition after 24 h (Fig. 4D). Pyruvate kinase (PK) activity profile was the inverse of that found for HK activity, with an increased activity 24 h after H₂O₂ exposure for both treatments (Fig. 4E). The activity of lactate dehydrogenase (LDH), an enzyme involved in anaerobic glycolysis, was lower within 2 h after challenge with either concentration of H₂O₂ compared with control conditions and

increased by 24 h after H₂O₂ exposure (Fig. 4F). Pyruvate carboxylase transcription was also investigated, presenting an increase 2 h after challenge with 2 mM H₂O₂, but not 4 mM, compared with control (Fig. 4G). At 24 h, however, the transcriptional level of pyruvate carboxylase had decreased in response to both oxidative challenges (Fig. 4G). Phosphoenolpyruvate carboxykinase (PEPCK) transcription increased under both H₂O₂ concentrations for 2 h and decreased to levels below that of the control condition 24 h later (Fig. 4H). The levels of G6P increased after H₂O₂ challenge in both treatments (Fig. 4I). Figure 4J summarizes the suggested pathway leading to the production of G6P, both by glucose uptake and gluconeogenesis. Subsequently, G6P is used for glycogen synthesis.

The ISP is involved in glucose uptake and glycogen metabolism. We confirmed that BME26 cells are responsive to insulin (Fig. 5B) and performed experiments using RNAi knockdown of the p85 Regulatory Subunit of PI3K (Fig. 5C). GS transcription increased after p85 knockdown (Fig. 5D), as did the glycogen levels (Fig. 5E). On the other hand, AKT knockdown (Fig. 5F) also increased GS transcription (Fig. 5G) but did not affect PEPCK transcription (Fig. 5H), whereas GSK3β knockdown (Fig. 5I) increased both GS and PEPCK transcription (Fig. 5, J and K).

Mitochondrial oxidative control is related to the carbohydrate metabolic compensation coupled to high tolerance to oxidative stress in tick cells

Anaerobic glycolysis is the main pathway responsible for supplying the cell with both ATP and NADH, usually associated with the Warburg effect. Therefore, we investigated a possible switch from oxidative to nonoxidative metabolism during oxidative challenge (Fig. 6). Representative traces of oxygen consumption by BME26 cells after exposure to H₂O₂ are shown in Figure 6A. The respiratory complex I transfers electrons from the NADPH into the electron transport chain. We measured the complex I coupled oxygen consumption rate (OCR) after inhibition of complex I with rotenone, which decreased after 2 h of H₂O₂ treatment at both concentrations, suggesting a reduction in the energy supply by the mitochondria (Fig. 6B). Of interest, the oxygen consumption coupled to ATP synthesis (ATP-linked respiration) was not altered by H₂O₂ treatment (Fig. 6B). The maximum respiratory rate of the electron transport system (ETS), induced by uncoupling of respiration, also was significantly decreased after H₂O₂ exposure (Fig. 6B). The spare respiratory capacity showed a similar profile, suggesting that, although ATP synthesis through oxidative phosphorylation is unchanged, the maximal capacity provided by the mitochondria is reduced, indicating a possible switch to non-oxidative metabolism during oxidative challenge (Fig. 6B). The mitochondrial morphology was accessed by MitoTracker Green staining, to observe mitochondrial change shape. H₂O₂ treatment indicates a dynamic morphological change (Fig. 6C), with a reduction of elongate mitochondrial shape (yellow arrow) and greater number of dotted mitochondria morphology (white arrows, yellow highlight square below). After silencing of NADPH-dependent isocitrate dehydrogenase (ICDH) (Fig. 7B),

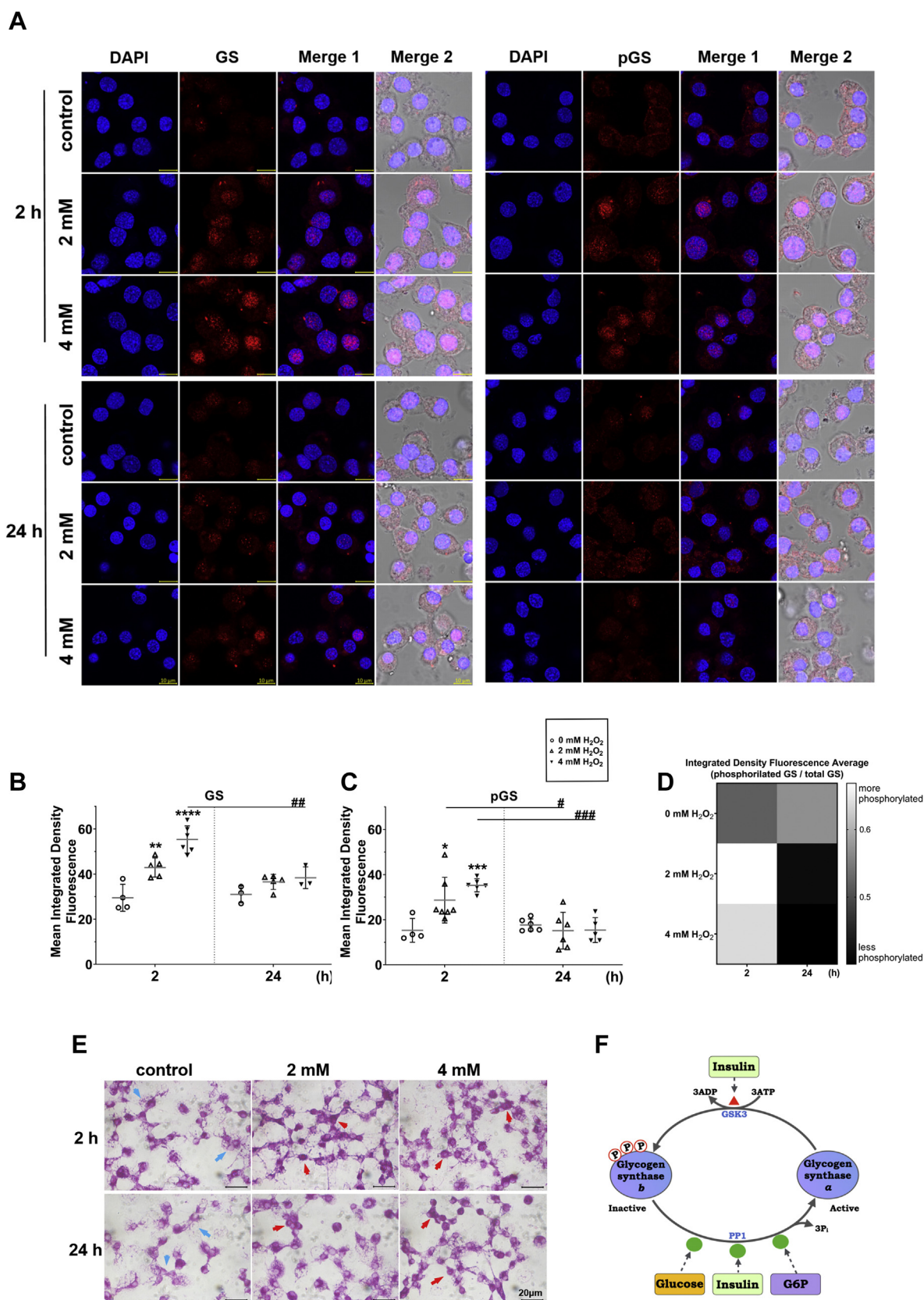


Figure 3. Glycogen metabolism regulation in BME26 cells upon H₂O₂ challenge. H₂O₂-tolerant BME⁶⁴¹ cells increased glycogen synthase protein expression 2 h after challenge with 2 or 4 mM H₂O₂. *A*, immunolocalization (red signal) of phosphorylated Ser⁶⁴¹ glycogen synthase (pGS) or total GS, as well as nuclei staining (blue signal), was performed after 2 or 4 mM H₂O₂ challenge, for 2 and 24 h. Images were captured in a confocal laser scanning microscope, LSM 710, Zeiss. The scale bar represents 10 μm. *B–D*, quantitative analysis of GS (*B*), pGS (*C*), and active GS (*D*). *E*, periodic acid–Schiff staining of BME26 cells after treatment with 2 and 4 mM H₂O₂ for 2 and 24 h. Blue arrows indicate diffuse staining and red arrows indicate perinuclear staining. Light

Redox imbalance remodels the tick glucose metabolism

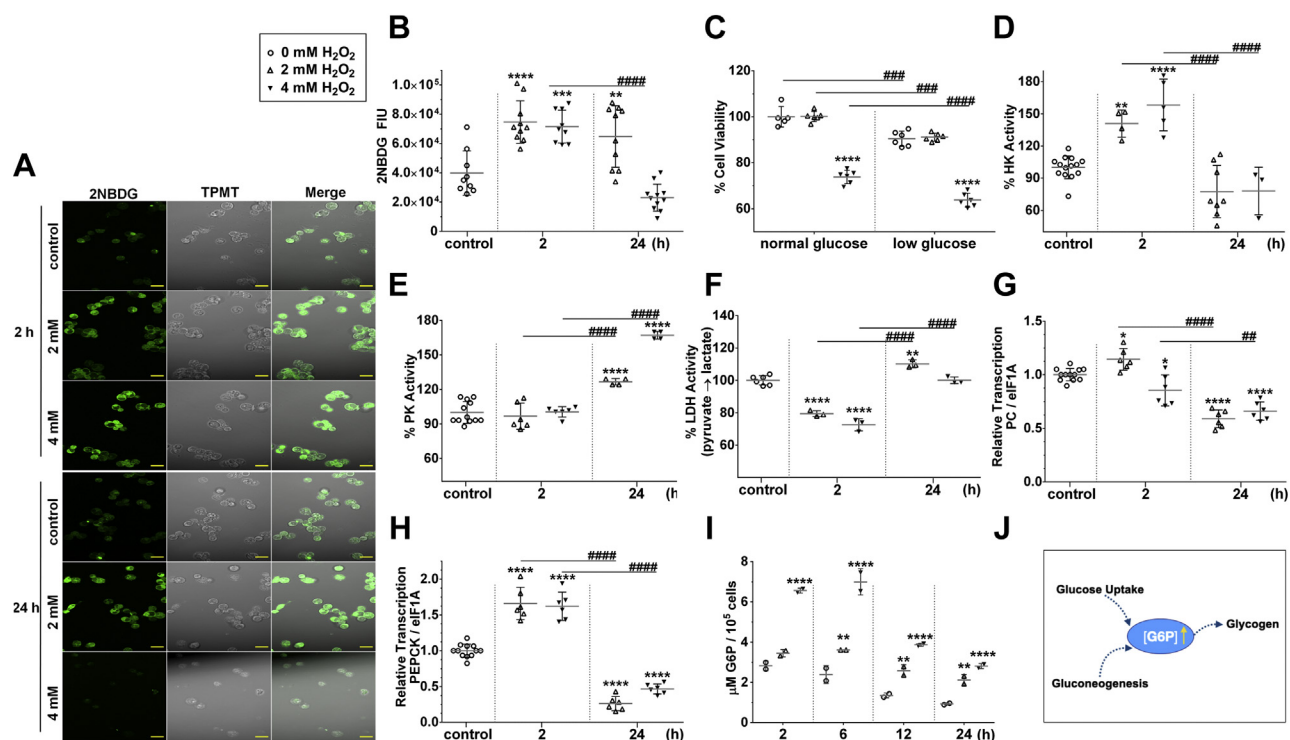


Figure 4. Gluconeogenesis is related to glycogen stores in H₂O₂-challenged BME26 cells. A, glucose analogue (2NBDG) uptake after either 2 or 4 mM H₂O₂ treatment for 2 or 24 h. The scale bar represents 20 μm. B, glucose uptake quantification based on A. C, BME26 cell viability (trypan blue exclusion) after 2 or 4 mM H₂O₂ challenge in normal or low-glucose media (see [Experimental procedures](#) for details). Enzyme activity for hexokinase (HK) (D), pyruvate kinase (PK) (E), and lactate dehydrogenase (LDH) (F) in BME26 cells in response to 2 or 4 mM H₂O₂ after 2- and 24-h exposure. Transcriptional analysis for pyruvate carboxykinase (PC) (G) and phosphoenolpyruvate carboxykinase (PEPCK) (H) in BME26 cells in response to 2 or 4 mM H₂O₂ after 2- and 24-h exposure. I, quantification of glucose 6-phosphate in BME26 cells over time after treatment with H₂O₂ (2, 6, 12, and 24 h). Experiments were performed with three independent biological samples in three experimental replicates each, where **p* < 0.05, ***p* < 0.01, ****p* < 0.001, *****p* < 0.0001, compared with control; and ##*p* < 0.01, ###*p* < 0.001, ####*p* < 0.0001, compared between the groups, in Tukey's multiple comparisons test. J, schematic depiction of increased G6P content (due to either increased glucose uptake or gluconeogenesis) toward glycogen formation.

cell viability is not reduced (Fig. 7A), but the transcription of glucose-6-phosphate dehydrogenase (G6PDH), GS, and PEPCK increased (Fig. 7, C–E). The supply of glycogen *via* gluconeogenesis and the compensatory relationship between G6PDH and HDI are shown in the diagram (Fig. 7F).

Discussion

A markedly increased consumption of glucose by tumors in comparison with the nonproliferating normal tissues was first described more than 90 years ago by the German physiologist Otto Warburg (34–36). However, tumor metabolism has only recently been recognized as a hallmark of cancer, becoming a topic of a renewed interest (17, 37). More than 90 years after the proposal that the Warburg effect is responsible for maintaining cancer cell homeostasis, many authors now consider this an essential phenomenon to support the metabolic demand in these cells (38). In addition, tumorigenesis is also dependent on changes in more complex cellular metabolism, involving genetic and interaction controls (39). Cancer-promoting changes include sustaining proliferative signaling,

evading growth suppressors, resisting cell death, enabling replicative immortality, inducing angiogenesis, and activating invasion and metastasis, which can result in the death of the organism (37).

Lactate is the product of pyruvate degradation in the cytoplasm. For a long time, it was believed to be produced only under hypoxia. Lactate production depends on many factors and is not influenced only by the lactic anaerobic system. In addition, large concentrations of lactate are present in neoplastic cells, even at rest, a phenomenon known as the Warburg effect, as discussed above, which can occur due to the high metabolic rate of tumor cells. Interesting, BME26 cells under oxidative H₂O₂ challenge presented short periods of increased lactate, which happened earlier (between 2 and 6 h) after 4 mM treatment than after 2 mM treatment (12 h) (Fig. 1C). Studies in *R. microplus* ticks indicate that there is a mutual regulation among major enzymes of glucose metabolism at the transcriptional and enzymatic levels (40). It was shown that gluconeogenesis makes a significant contribution to maintain the energy balance in the late stages of *R. microplus*

microscope images were captured in bright field using Axio Scope.A1, Zeiss polarized light microscope through the Blue Zeiss software. The scale bar represents 20 μm. Analyses were performed on three independent biological samples with three experimental replicates. F, schematic depiction of glycogen synthase activity regulation in vertebrates, which is downregulated by phosphorylation (including at Ser⁶⁴¹) *via* GSK3β (inhibited *via* insulin signaling), while glucose and glucose 6-phosphate upregulate GS activity in an allosteric fashion, and by PP1-mediated dephosphorylation (prompted by insulin signaling).

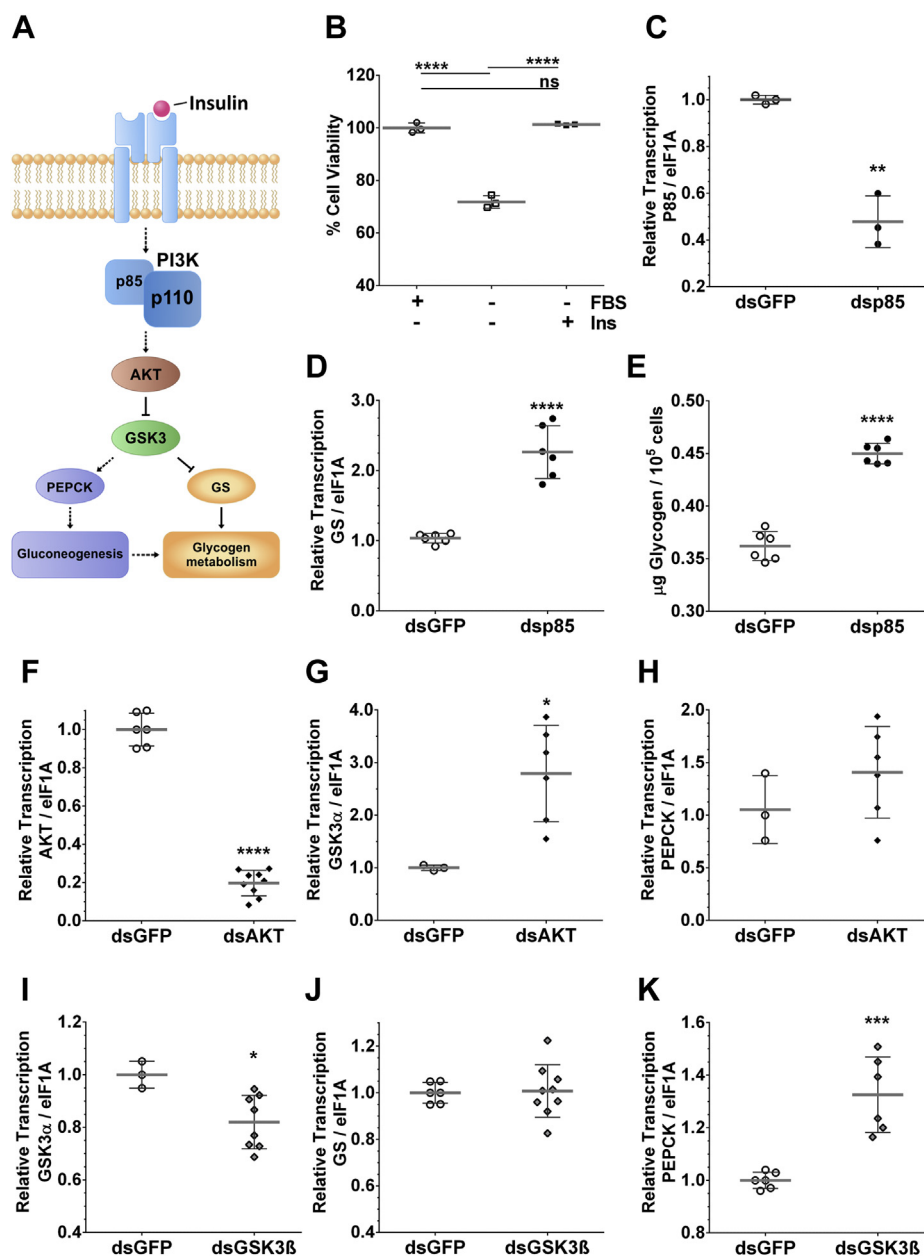


Figure 5. The conserved axis of insulin pathway is closely correlated to glycogen metabolism and gluconeogenesis in BME26 cells. A, partial schematic depiction of the insulin signaling pathway and its contribution to glycogen metabolism. Indicated components were further analyzed. *Straight arrows*, single-step process; *dotted arrow*, multistep process; *arrowhead*, activation; *blunt arrowhead*, inhibition. B, BME26 cells respond to the addition of exogenous insulin (400 nM), recovering the viability lost by removing fetal bovine serum for 24 h (C) PI3K regulatory subunit (p85) gene silencing validation and its effects on glycogen synthase (GS) transcript levels (D) and glycogen content (E). Protein kinase B (AKT) and GSK3 β gene silencing validation (F and I, respectively), and its effects on GS (G and J) and PEPCK (H and K) transcript levels, respectively.

and *A. aegypti* embryo development (41–43). In this case, these arthropods use nonglycosidic compounds, such as lactate and amino acids, to resynthesize glycogen through gluconeogenesis. These findings suggest that glucose may form a wide range of substrates through this pathway, ensuring precursors are available for biosynthesis processes. The enzyme GS works primarily to regulate glycogen synthesis (Fig. 2E). An increase in GS transcription level was observed in BME26 cells challenged with 2 mM H₂O₂ (Fig. 2A). In addition, the transcription of GSK3 β , a regulator of GS, decreased after treatment with H₂O₂ at 2 mM, but not 4 mM (Fig. 2B). The transcription of enzymes

involved in glycogen degradation, such as phosphoglucose isomerase and GDE, also increased under 2 mM of H₂O₂ at 2 h, followed by a decrease at 24 h (Fig. 2, C and D). Previously published data show that *R. microplus* metabolism is responsive to and dependent on insulin signaling (16). Furthermore, the amount of GS (Fig. 3, A and B) and pGS (Fig. 3, A and C) increased in response to H₂O₂ challenge, specially at 2 h of exposure. However, the pGS/GS ratio reveals an increase in unphosphorylated GS, the active form of the enzyme, after 24 h at both H₂O₂ concentrations tested and as early as 2 h after challenge at the highest concentration (Fig. 3D), suggesting that

Redox imbalance remodels the tick glucose metabolism

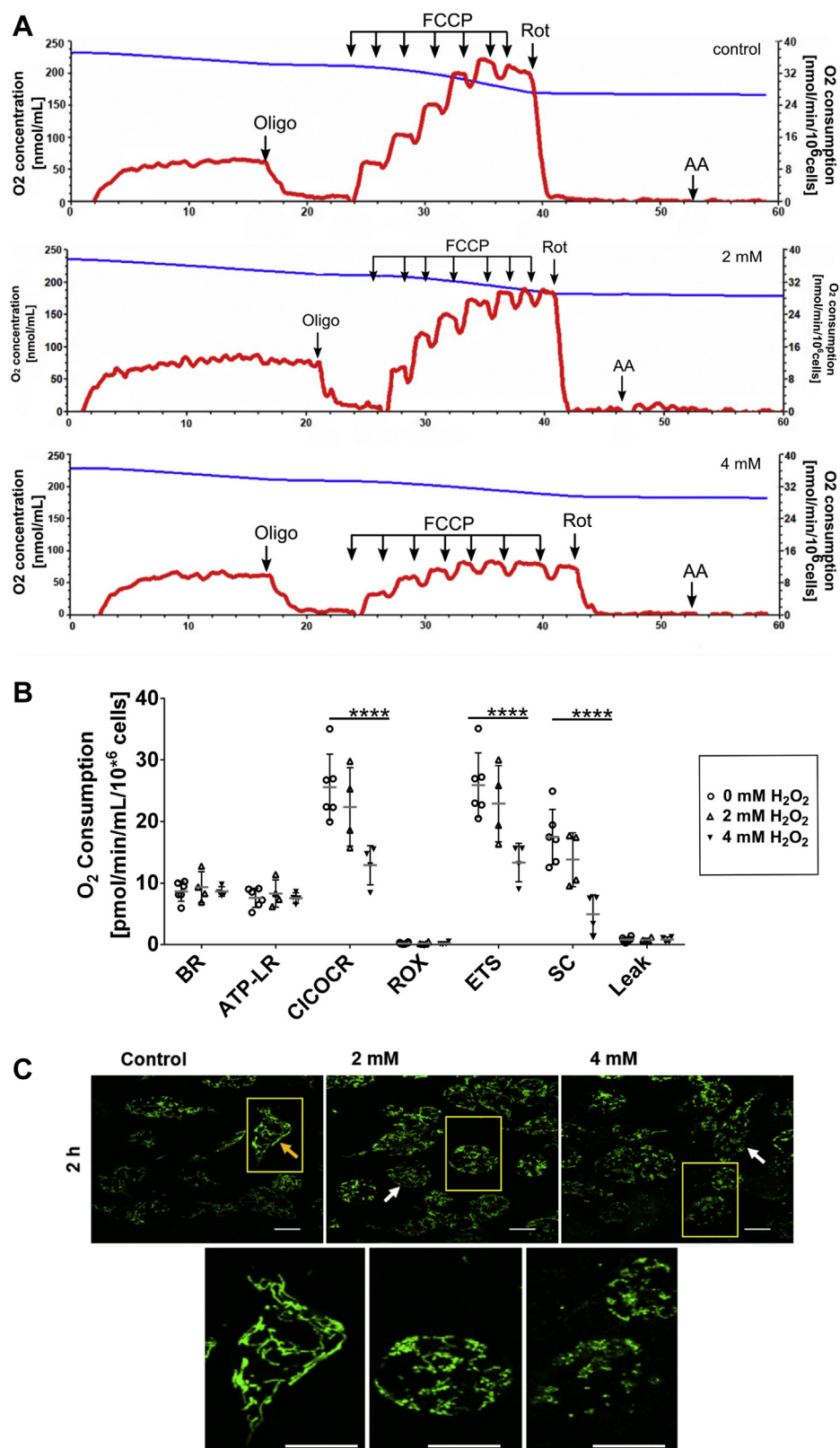


Figure 6. Decrease in mitochondrial respiratory rates induced by H₂O₂ treatment on BME26 cells. *A*, typical traces of oxygen consumption rates (OCR, red line) and oxygen concentration (blue line) of BME26 cells after treatment with 2 and 4 mM H₂O₂ for 2 h. *B*, oxygen consumption rates from BME26 cells (open circle), and after treatment with 2 (open triangle up) or 4 mM (triangle closed down) H₂O₂ for 2 h. Data are expressed as mean ± standard deviation (SD) of five different experiments. Comparisons between groups were done by two-way ANOVA for repeated measurements and *a posteriori* Holm–Sidak test, adjusted for multiple comparisons ($p < 0.001$). *C*, fluorescence images of mitochondrial membrane of BME26 cells stained with 200 nM MitoTracker Green ($\lambda_{ex} = 488$ nm, $\lambda_{em} = 500$ –530 nm) after 2-h oxidative challenge. Yellow boxes indicate a digital zoom of one cell. Yellow arrow shows mitochondria elongated shape, whereas white arrows show dotted mitochondria shape. The scale bar represents 100 μ m.

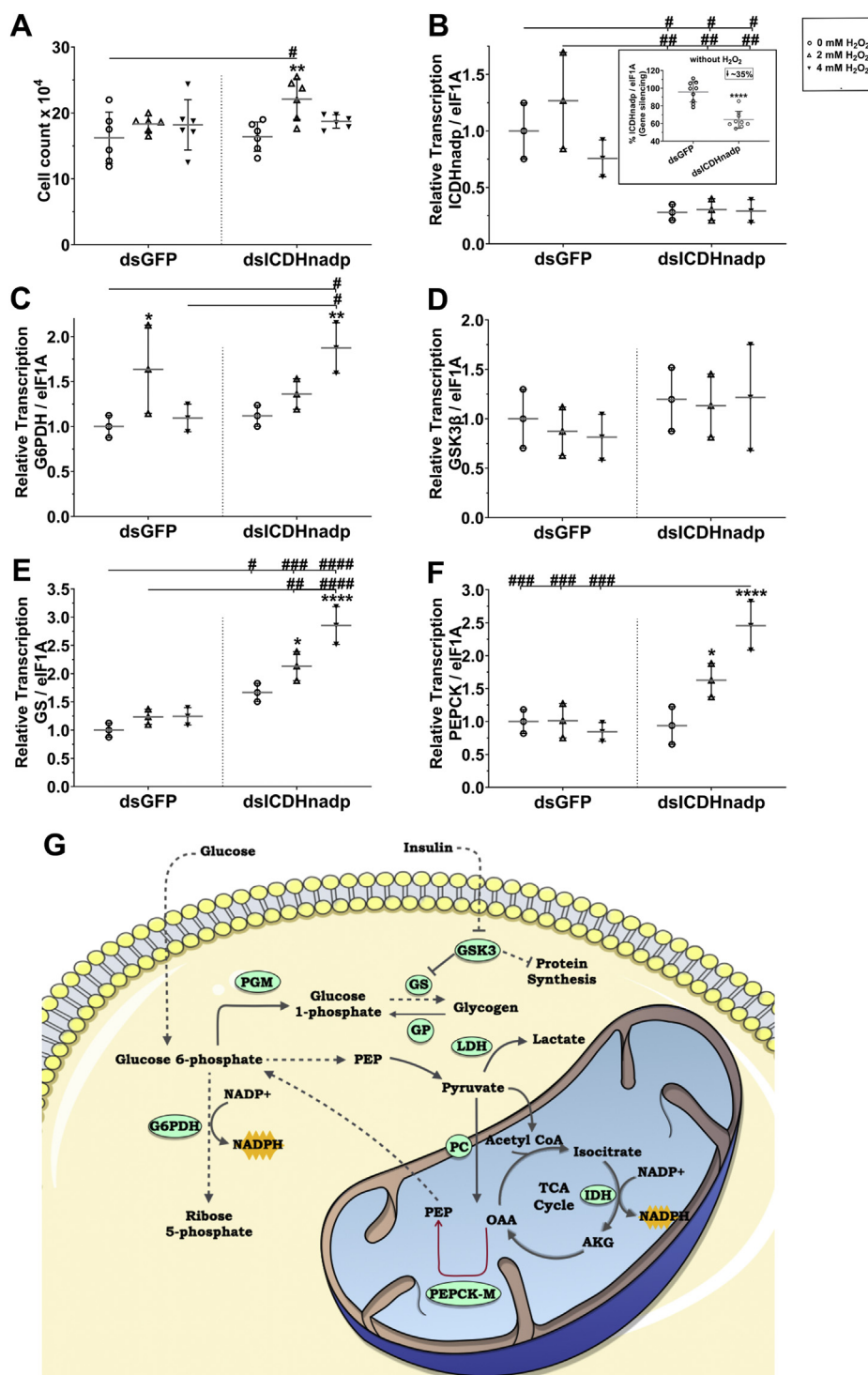


Figure 7. Metabolic remodeling involves simultaneous gluconeogenesis and mitochondrial activity in BME26 cells. A, viable NADP-ICDH knocked down BME26 cells after H₂O₂ treatment. B, NADP-ICDH gene silencing validation and its effects on the transcript levels of glucose-6-phosphate dehydrogenase (G6PDH) (C), glycogen synthase kinase 3 β (GSK3β) (D), glycogen synthase (GS) (E) and phosphoenolpyruvate carboxykinase (PEPCK) (F), as measured 2 and 24 h after 2 or 4 mM H₂O₂ addition, in BME26 cells. G, schematic representation of the proposed metabolic remodeling in BME26 in response to H₂O₂ challenge. **p* < 0.05; ***p* < 0.01; *****p* < 0.0001; compared with the control without H₂O₂ within each H₂O₂ concentration of same dsRNA treatment; and #*p* < 0.05; ##*p* < 0.01; ###*p* < 0.001; ####*p* < 0.0001 compared with dsRNA nonrelated (dsGFP) within dsICDHnarp gene silencing, in Tukey's multiple comparisons test.

glycogen metabolism is activated. The glycogen staining follows the same profile, increasing with the oxidative challenge (Fig. 3E). The increase in the phosphorylation of serine 9 on GSK3β (inhibited enzyme) after H₂O₂ challenge corroborates

with the increased GS activity (Fig. S3). Thus, glycogen resynthesis is likely being activated in response to H₂O₂ in BME26 cells, suggesting that *R. microplus* tick cells perform a metabolic adaptation that leads to tolerance while maintaining

Redox imbalance remodels the tick glucose metabolism

redox balance. Moreover, BME26 cells have been previously shown to be responsive to insulin signaling (16), and we have successfully used insulin as a positive control in 2-NBDG internalization experiment (31).

Glucose supply is required to support glycogen synthesis. There is also a correlation between glucose uptake and increased glycogen content after H₂O₂ challenge, as demonstrated here (Fig. 4, A and B). The redox imbalance led to increased glucose uptake in BME26 cells, and the enzyme responsible for glucose phosphorylation, HK, responded by increasing its activity after 2 h of exposure to H₂O₂ at both concentrations (Fig. 4D). PK, a glycolysis regulator that acts downstream of HK, also increased its activity within 24 h of exposure to both H₂O₂ concentrations (Fig. 4D). Therefore, glucose may be the key substrate that drives this metabolic adaptation in BME26 cells during redox imbalance, since glycolysis appears to be accelerated after H₂O₂ challenge and glucose uptake is high under this same condition. In fact, cell viability was significantly lower at low glucose concentrations when challenged with 4 mM H₂O₂ (Fig. 4C), and LDH activity increases at the same time point when PK activity increases (Fig. 4E). Characteristic of the Warburg effect, an increased glucose uptake supports an anaerobic glycolysis, producing lactate as a cellular by-product (44). The lactate generated in this process can contribute to the synthesis of glucose through gluconeogenesis, as described in Exton and Park (45). Moreover, pyruvate carboxylase, which catalyzes one of the first steps of gluconeogenesis, showed increased transcription at 2 mM H₂O₂ after 2 h. Thus, we investigated the transcription of PEPCK, which plays a key role in energy homeostasis because it is involved in the regulation of fatty acid re-esterification, glucose synthesis, transamination, and the cataplerosis of citric acid cycle anions (46). It is well established that changes in PEPCK gene transcription regulate the total activity of this enzyme (46, 47). Further assessing the involvement of gluconeogenesis in the oxidative challenge response, we observed an increase in the relative transcription of PEPCK at 2 h after H₂O₂ addition for both concentrations (Fig. 4G). Concomitantly, pyruvate carboxylase transcription increased, suggesting an activation of gluconeogenesis to support the accoupling of glucose and glycogen synthesis (Fig. 4I). On the other hand, the amount of G6P did not change after H₂O₂ challenge (Fig. 4H), suggesting that the synthesis and mobilization of this substrate remain constant.

Such mechanisms are classically known to be regulated by insulin, especially in mammals (48). In the BME26 cells, the viability was significantly reduced in the absence of insulin or fetal bovine serum but increased in the presence of either treatment (Fig. 5B), strongly indicating the presence of an insulin-responsive system in BME26 cells, as suggested by Abreu *et al.* (16). To investigate whether the regulation of glycogen metabolism and gluconeogenesis in BME26 cells are also dependent on the insulin signaling cascade, we used gene silencing of the p85 protein, the regulatory subunit of PI3K. The metabolic response to insulin is mediated primarily by PI3K (49). Thereby, in the presence of insulin, the formation of the IRS complex promotes the recruitment and activation of

class IA PI3K (Fig. 5A). When the insulin receptor or the IGF receptor is inactive, the p85 regulatory subunit stabilizes and maintains the p110 catalytic subunit in a state of low activity (50). Accordingly, after p85 knockdown in BME26 cells (Fig. 5C), GS transcription, as well as glycogen content, increased (Fig. 5, D and E). The same effect of increased GS transcription was observed after knockdown of another ISP component, AKT, with no effect observed on PEPCK transcription (Fig. 5, F–H). In the case of GSK3β knockdown (Fig. 5I), both GS and PEPCK transcription were induced (Fig. 5, J and K), suggesting the control of glycogen metabolism mediated by GSK3β and, surprisingly, an indirect genetic regulation of the gluconeogenesis pathway through GSK3β. Other studies suggest an indirect genetic regulation of the gluconeogenesis pathway through GSK-3 (40), with PEPCK expression control being mediated by GSK-3 in mammalian cells (51). At the enzymatic level, GSK3β is regulated by phosphorylation, and a 15% suppression may not affect the metabolism substantially overall. Effectively, the low rate in GSK3β silencing afforded analysis of the effect of GSK3β reductions on the transcription of gluconeogenesis genes. Given the conservation of these pathways of carbohydrate metabolism, and the high glycolytic activity observed after H₂O₂ treatment, we were prompted to investigate the mitochondrial contribution in BME26 cells responding to oxidative challenge.

Recently, we described the tolerance, survival, proliferation, and adaptability of *R. microplus* embryonic cell line BME26 to an oxidative challenge. In this context, a comparative analysis was performed with different cell types regarding their survival to H₂O₂ (31). Figure 1A presents an explanatory graph with the viability of different cell lines used for comparative tests of H₂O₂ susceptibility. We demonstrate that the arthropod embryonic cells tested (S2, BME26, and Aag2) display a higher H₂O₂ tolerance compared with mammalian cells, when subjected to treatment between 62.5 and 2000 μM H₂O₂. BME26 and S2 cells showed a similar pattern of cell viability, being acutely tolerant to the oxidative challenge induced by H₂O₂. Viability of S2 cells was affected only to about 20% at the highest tested concentration of 2 mM H₂O₂. However, Aag2 cells exhibited an increase of about 30% in cell numbers, at the lowest concentrations of 125 to 250 μM H₂O₂. Cytotoxic effects were observed at concentrations above 1000 μM (1 mM) H₂O₂, with about 20% lethality. Therefore, 24 h after H₂O₂ addition, it was possible to observe that the tested embryonic arthropod cell lines tolerate higher H₂O₂ concentrations than some mammalian cell lines in this experiment, as well as others reported in the literature. This surprising discovery opened up our perspective to look at the "good side" of ROS for cellular metabolism.

ROS are natural by-products of metabolism that have toxic effects associated with tissue injury and many pathological processes, including septic shock (52, 53). However, we live in an oxygen-rich environment and ROS and their chemical reactions are part of the basic chemical processes of normal metabolism (54). Accordingly, organisms have evolved sophisticated mechanisms to control these reactive molecules (55). In the last 2 decades, it has become increasingly evident

that ROS also play a role in the regulation of many intracellular signaling pathways that are important for normal cell growth and inflammatory responses that are essential for host defense (55–58). We hypothesize that H₂O₂ triggers a metabolic adaptation *via* gluconeogenesis switching from transamination to glycogen storage. At the same time, increasing glucose uptake maintains glycolytic pathways for energy supply, as well as pentose phosphate pathway for NADPH production. Accordingly, we observe metabolic changes leading to glycogen accumulation in arthropod embryonic cell lines after oxidative challenge. The great metabolic plasticity, also known as metabolic remodeling, generates a high energy demand. Our temporal analysis of glycogen content in BME26 cells shows a tendency to accumulate glycogen 6 h after H₂O₂ bolus addition (at 2 or 4 mM), keeping glycogen levels high up to 24 h (Fig. 1B) and reverting to control levels after 48 h (Fig. S1). Aag2 cells, on the other hand, which are slightly less tolerant to H₂O₂ than BME26 cells, showed an increase in glycogen 6 and 12 h after challenge with H₂O₂ at 2 mM, but not at 1 mM (Fig. S2). The similar pattern of cell viability, being acutely tolerant to the oxidative challenge induced by H₂O₂, involving the glucose metabolism adaptation is usually described in cancer cells.

The electron transport chain is one of the stages of cellular respiration, characterized by the transport of electrons in a compilation of molecules fixed on the inner membrane of the eukaryotic cell mitochondria, toward a final electron acceptor, in several energy-releasing steps for ATP synthesis (59). Thus, the flow of electrons in the respiratory chain is carried out through a redox spectrum from NAD⁺/NADH to O₂/H₂O, passing through four large protein complexes. Inhibitors of these complexes were used in order to investigate oxidative metabolism in BME26 cells (Fig. 6A). After treatment with 2 and 4 mM H₂O₂, the rates of complex I-coupled OCR, ETS, and spare capacity were significantly affected (Fig. B). Beyond this response to H₂O₂, change in mitochondrial shape was observed after either treatment (Fig. 6C). These results suggest a shift from oxidative to nonoxidative metabolism, corroborating with data on increased enzyme activity of PK and LDH (Fig. 4, D and E), similar to that observed in the Warburg effect. However, unlike with the Warburg effect, glycogen reserves are not being mobilized under these conditions, but increase in amount. Thus, the data suggest that glycogen synthesis is maintained by gluconeogenesis (Fig. 4, F and G) after redox challenge, which uses lactate and pyruvate to synthesize glucose that will be incorporated into glycogen.

In previous studies, after G6PDH knockdown in BME26 cells, a cellular environment was induced by oxidative stress in which NADP-ICDH seems to be a compensatory NADPH provider (31). Here, after NADP-ICDH knockdown (Fig. 7B), it is possible to observe the opposite reaction, with an increase in G6PDH transcription (Fig. 7C) without affecting cell viability (Fig. 7A). The interactions between NADPH-producing enzymes (G6PDH, NADP-ICDH) under different stress conditions, such as oxidative stress, starvation, and desiccation, has been evaluated in *Drosophila*. The results showed that NADPH production was mostly afforded by

G6PDH and NADP-ICDH, which were more accentuated in oxidative stress (60), suggesting that both enzymes work together to maintain the oxidative balance. In the case of NADP-ICDH, GS also increased its transcriptional level, as well as PEPCK (Fig. 7, E and F). According to these results, BME26 cells treated with H₂O₂ induce gluconeogenesis as an adaptive compensation strategy, involving NADP-ICDH, G6PDH, and PEPCK enzymes (Fig. 7G).

A great progress has been achieved with arthropod model systems to study various human disorders including diabetes, multiple sclerosis, epilepsy, and cancer (8, 61–63). Thus, arthropod cell lines act as excellent experimental models to study physiology, gene regulatory networks, metabolic fluxes, and the regulation of energy homeostasis (15, 32, 64–68). The present work demonstrates that ticks are able to support high H₂O₂ concentrations and perform an adaptive response to H₂O₂ involving glucose metabolism, where tolerance is linked to metabolic control in eukaryotic cells. Moreover, this study helps to elucidate an adaptive mechanism developed by BME26 cells under H₂O₂ exposure to maintain cellular performance and redox balance and also contributes to a better understanding of arthropod physiology and metabolism.

Experimental procedures

Cell lines

Glucose metabolism remodeling was investigated in the BME26 cell line. In addition, other invertebrate and vertebrate cell lines were challenged with H₂O₂ prior to cell viability determination (S2, LLCMK2, and macrophage). Furthermore, glycogen and lactate contents in BME26 and Aag2 cell lines were compared upon H₂O₂ treatment. The same selection of cell lines was previously studied in our laboratory and were kept as described (31).

H₂O₂ treatment procedures

Hydrogen peroxide treatment was performed with a single bolus addition (33). To assess cell susceptibility, cells were incubated with H₂O₂ concentrations ranging from 0 to 2 mM, and cell viability was checked 24 h after treatment. Lethal dose to reduce BME26 cell viability by 25% (LD₂₅) was estimated by treatment with H₂O₂ ranging from 0 to 8 mM, for 24 h. Further tests with BME26 cells used H₂O₂ concentrations of 2 and 4 mM based on our previous observations (31), with incubations at the indicated intervals. BME26 cells were used between passages 40 and 60.

Cell viability assays

Cell viability was determined using a Neubauer hemocytometer with 0.04% Trypan Blue (Sigma-Aldrich) exclusion technique and visual detection (69). The experimental procedure and calculations were done according to standard methodology as reported (31). The number of viable cells was counted directly on hemocytometer under a light microscope (Axio Imager 2, Zeiss) or on images captured with an AxioCam 503 color camera using the cell counter Manual Counting plugin on ImageJ software (70).

Redox imbalance remodels the tick glucose metabolism

Alternatively, cell viability was measured using the tetrazolium dye 3-(4,5-dimethylthiazol-2-yl)-2,5-diphenyltetrazolium bromide (MTT) colorimetric assay performed on 24-well plates (16, 31). Unless otherwise stated, absorbance values (570 nm) of control condition were used for normalization (100% viability) to determine cell viability.

Glucose analogue uptake in BME26 cells

D-Glucose fluorescent analogue 2-NBDG {2-[N-(7-nitrobenz-2-oxa-1,3 diazol-4-yl)amino]-2-deoxy-d-glucose} (Molecular probes, #N13195) was used as an indicator for direct measurement of glucose uptake (71), as reported for BME26 cells (31). Cells were allowed to adhere on a clear confocal dish (SPL Lifesciences, model 200350) for 24 h in complete medium. Cells were then washed twice with 500 μ l of L15B300 medium without glucose supplementation [L15 (-) glucose]. Cells were further incubated in 500 μ l of L15 (-) glucose for either 2 or 24 h with H₂O₂ at 2 or 4 mM. The glucose analogue, 2-NBDG, was added to the growth medium in the last 90 min of H₂O₂ challenge, at 100 μ M final concentration, and the plate was kept at 34 °C in the dark. After two washes with 500 μ l of L15 (-) glucose, live cells were observed under a confocal microscope (Zeiss LSM710). An additional positive control for 2-NBDG uptake was done with exogenous bovine insulin addition. Cells were cultured for 24 h to adhere on round glass coverslip and washed twice with L15 (-) glucose. Then, 100 μ M of 2-NBDG was added to the growth medium, followed by 1 μ M bovine insulin, and incubated for 1 h. Images were taken using Zeiss LSM710 confocal microscope, with a 40x magnification objective (Water Plan-Apochromat 40x/1.0 DIC) Ex. 488 nm; Em. 520 nm using the ZEN 2.3 program (black edition). Quantification of the mean fluorescence intensity per cell area in mm² was determined with ZEN 2.3 (blue edition) software (Carl Zeiss Microscopy GmbH, 2011).

Total and Ser⁶⁴¹-phosphorylated glycogen synthase immunolocalization

BME26 cells were challenged with H₂O₂ (at 2 or 4 mM, for 2 or 24 h) in 24-well plates with a round glass coverslip at the bottom of each well. After treatment, cells were washed twice with PBS pH 7.0 and fixed in 4% paraformaldehyde solution (in PBS pH 7.0) for 25 min at room temperature, then washed twice with PBS pH 7.0. Permeation was done in ice-cold acetone for 3 min, followed by five washes in PBS. Cells were kept for 1 h in blocking solution (1% bovine serum albumin in PBS), followed by a 16-h incubation at 4 to 8 °C with the respective primary antibody, anti-Glycogen Synthase (GS, total) (Cell signaling, #3893) or anti-Glycogen Synthase phosphorylated at Ser641 (pGS, inhibited) (Cell signaling, #3891), at 1:200 dilution in blocking solution. After that, cells were washed three times, incubated with secondary anti-rabbit IgG antibody conjugated to AlexaFluor 555 (Cell signaling, #4413), diluted 1:1000 in blocking solution, for 2 h, followed by incubation with DAPI (1 μ g/ml) for 15 min. Round coverslips were prepared in glycerol, after two washes, and observed

under microscope. Images were taken using Zeiss LSM710 confocal microscope, with a 40x magnification objective (Water Plan-Apochromat 40x/1.0 DIC) and Ex: 555 nm, Em: 565 nm.

Glycogen staining

After H₂O₂ treatment, cells in round glass coverslips were fixed in 4% paraformaldehyde solution, for 25 min. Carbohydrates were oxidized in periodic acid solution for 5 min, followed by two washes in running water. Schiff reagent was added for 5 min, and washed three times with distilled water. A subsample of coverslips was used to locate cell nuclei by staining with Harris hematoxylin solution for 6 min and rinsed in running water for 5 min. For assembly, coverslips were dehydrated and clarified through 95% ethanol, absolute ethanol, and xylene, two exchanges of 2 min each, and then assembled in Entellan mounting medium. All steps were performed at room temperature. Images were captured in bright field microscopy using polarized light, 20x magnification, in an Axio Scope.A1 microscope (Zeiss) with the Blue Zeiss software.

Mitochondria staining

The green-fluorescent mitochondrial stain, MitoTracker Green (Molecular probes, Invitrogen, #M7514), was used to verify the mitochondrial location. The entire procedure was performed according to the manufacturer. After 2 or 4 mM H₂O₂ treatment, for 2 h, adherent cells on a clear confocal dish (SPL Lifesciences, model 200350) were washed once with 500 μ l of prewarmed L15 complete medium and incubated with 500 μ l of 200 μ M MitoTracker Green, diluted in complete medium, for 20 min at 34 °C in the dark. After three washes with complete medium, cells were observed by confocal microscopy. Image acquisition was performed using the Zeiss LSM710 confocal laser scanning microscope, using objective 63x magnification (LD plan-neofluar 63x/1.0 DIC), through the program ZEN 2.3 (black edition).

Protein, glycogen, lactate, and glucose 6-phosphate quantification

The total protein concentration was determined using the Bicinchoninic Acid Kit (Sigma-Aldrich Product # BCA-1) according to the manufacturer's instructions, with bovine albumin as standard (72).

The glycogen content was determined in 250 μ l of extraction buffer (200 mM sodium acetate buffer, pH 4.8; 0.1% Triton-X100; protease inhibitor cocktail, Sigma Aldrich #P8340) after cells were mechanically disrupted by vortexing and 20 iterations of passing through a 26G needle in a 1-ml syringe. After centrifugation at 12,000g for 10 min, 40 μ l of supernatant aliquots were incubated with 1 U of α -amylglucosidase (Sigma-Aldrich #A7420), at 40 °C for 4 h, after which glucose concentration was measured by the glucose oxidase method using a commercial kit (Labtest Ref.133). Free glucose was measured in samples without α -amylglucosidase and subtracted from the results, and a standard curve was

generated to calculate glycogen levels in the samples (43). The glycogen content was normalized by the number of cells.

The lactate content was enzymatically determined with a colorimetric assay (Labtest Diagnóstica S.A. ref 138) following manufacturer instructions, using 20- μ l sample aliquots (or water for blank, or standard for positive control) in a final volume adjusted to 200 μ l in a 96-well microplate. Briefly, lactate oxidase generates pyruvate and H_2O_2 , and the latter is coupled in a peroxidase reaction to generate a product with maximal absorbance at 550 nm. The assay was performed at 37 °C for 5 min. Samples were read in a spectrophotometer (Multiskan Go Thermo Scientific) to determine the lactate concentration.

The G6P content was determined using EnzyChrom™ Glucose 6-Phosphate Assay Kit (EG6P-100). Cell samples (2×10^6) were homogenized in 100 μ l PBS and centrifuged at 12,000g for 5 min. Cleared supernatant aliquots (20 μ l) and G6P standard curve ranging from 0 to 1000 μ M were diluted in a premix solution and used for assay in 80 μ l of working reagent (100 μ l final volume), in a 96-well plate, according to the manufacturer's instructions. Briefly, G6P is oxidized by G6PDH and the generated NADPH is coupled to the WST-8 formazan chromogen. The intensity of the product color, measured at 460 nm, is proportional to the G6P concentration in the sample and was determined following manufacturer's instructions.

Enzymatic activities

Hexokinase (HK) activity was determined after treatment with H_2O_2 , using cell homogenates in 20 mM Tris-HCl, pH 7.5, containing 6 mM $MgCl_2$, 1 mM ATP, 0.5 mM NAD⁺, and 10 mM NaF. The enzymatic reaction was initiated with 2 mM glucose. Newly formed G6P was indirectly measured by adding an equal volume of 1 unit/ml of G6PDH from *Leuconostoc mesenteroides* (Roche #10127655001) and 0.3 mM of β -NAD⁺, in 700 μ l final volume. The production of β -NADH was determined at 340 nm, 30 °C (UVmini-1240 UV-Vis Shimadzu) using a molar extinction coefficient of 6.22 M^{-1} , as described (40). The enzymatic activity was normalized based on the total protein quantification and expressed in U/mg of total protein. The activity was calculated as a percentage of the activity under control conditions, which was set to 100%.

For measurement of pyruvate kinase (PK) activity, 30 μ l of cell homogenate was assayed in Tris-HCl buffer 20 mM pH 7.5, $MgCl_2$ 5 mM, ADP 1 mM, NADH 0.4 mM, and 1 U/ml of LDH. The reaction was initiated with phosphoenolpyruvate 1 mM, in 700 μ l final volume. The consumption of β -NADH was evaluated spectrophotometrically (UVmini-1240 UV-Vis Shimadzu) at 340 nm, 25 °C, using a molar extinction coefficient of 6.22 M^{-1} as described above (40). The enzymatic activity was normalized based on total protein quantification and expressed in U/mg of total protein. The activity was calculated as a percentage of the activity under control conditions, which was set to 100%.

LDH activity was determined kinetically using a colorimetric kit (Labtest Diagnóstica S.A. ref 86) following manufacturer's instructions. The activity was measured in 20- μ l

sample aliquots in a final volume of 200 μ l in a 96-well microplate. Briefly, LDH present in samples oxidizes NADH and the reaction is monitored spectrophotometrically at 340 nm in 1-min intervals at 37 °C to evaluate reaction linearity.

Respirometry analysis on BME26 cells after H_2O_2 treatment

Respiratory activity was measured using a two-channel titration injection respirometer (Oxygraph-2k, Oroboros Instruments), calibrated with PBS at 28 °C. Following treatment with H_2O_2 (2 or 4 mM for 2 h), or control condition, cells were harvested with trypsin solution (0.25% trypsin), counted, and suspended in PBS. Treated and control cells were placed into the O₂K chamber at a concentration of about 1×10^6 /ml and were incubated with continuous stirring at 750 rpm for about 10 min. Assay was performed at 28 °C and 750 rpm, started by adding 1 μ M oligomycin, and the oxygen consumption coupled to ATP synthesis (ATP-linked respiration) was calculated by subtracting the oxygen consumption after the addition of ATP synthase inhibitor from basal respiration rates. The maximum uncoupled respiration was assessed by stepwise titration of carbonyl cyanide p-(trifluoromethoxy) phenylhydrazone (FCCP) to reach a final concentration of 50 nM. Next, the contribution of complex I to electron flow was determined by the addition of 0.3 μ M of rotenone and calculated by subtracting FCCP-stimulated oxygen consumption from rotenone-resistant oxygen consumption. Finally, respiratory rates were inhibited by the injection of 1 μ g/ml antimycin A. The residual oxygen consumption represents the oxygen consumed by the cells, not due to respiration. The maximum respiratory rates (ETS) were calculated by subtracting the antimycin-resistant oxygen consumption from FCCP-stimulated oxygen consumption rates. The spare capacity is the amount of extra ATP that could be produced by oxidative phosphorylation in case of increased energy demand and was calculated by subtracting FCCP-stimulated oxygen consumption rates from basal respiration rates. The leak respiratory state, representing oxygen consumption in the presence of substrates but in the absence of ATP synthesis, was calculated by subtracting the oligomycin- from the antimycin-resistant oxygen consumption. All oxygen consumption rates were normalized per 1×10^6 cells/ml.

RNA isolation, real-time quantitative PCR, and relative quantification analyses

BME26 cells were harvested after treatment from 24-well plates for total RNA isolation using Trizol reagent (Invitrogen) according to the manufacturer's instructions. One microgram of total RNA was reversely transcribed with cDNA High-Capacity cDNA Reverse transcription kit (Invitrogen). The relative transcription was analyzed with cDNA template in a StepOne Plus platform (Applied Biosciences), with previously described primers (31, 40). Serially diluted cDNA samples from controls were used to construct a calibration curve. Amplification efficiencies between 85% and 100% were determined for each set of primers in 10- μ l reactions. The relative expression was determined using C_p values of each run

Redox imbalance remodels the tick glucose metabolism

in the Relative Expression Software Tool table (73). The *R. microplus* elongation factor- α (Elf1A) gene was used as a reference gene (74) to normalize the reactions. Relative expression of the calibrators was assigned the value of 1 unit. The statistical calculations (mean and standard deviation) were performed with data from three independent experiments in triplicates.

Double-stranded RNA synthesis and gene knockdown by RNA interference

cDNA from BME26 cells was used as template for dsRNA synthesis, using the RiboMAX Express RNAi System Kit (Promega) with previously described primers (31). dsRNA was purified according to the manufacturer's instructions, the concentration was determined spectrophotometrically at 260 nm, and an aliquot was used to check dsRNA integrity by 1% agarose gel electrophoresis stained by ethidium bromide and visualized in a transilluminator. A nonrelated dsRNA sequence coding for *Escherichia coli* GFP was used as a negative control for RNAi-induced gene knockdown. The size of the G6PDH dsRNA synthesized complex was 553 bp and that of the ICDHNADPH dsRNA was 565 bp (31). Specific primers were designed based on *R. microplus* sequences (31).

Double-stranded RNA was directly administered to BME26 cells kept on 24-well plates, as described (16). Three days after the addition of dsRNA, the cells were collected for testing. G6PDH gene silencing was confirmed by real-time quantitative PCR as well as by enzyme activity assay. To verify the persistence of G6PDH gene silencing after the first 3 days, the culture medium was fully replaced by 500 μ l of complete medium and incubated for a further 72 h. The cells were then collected for G6PDH enzyme activity (extended exposure assay, 6 days after the addition of dsRNA). For the H₂O₂ challenge, BME26 cells had their medium replaced (500 μ l) 3 days after the addition of dsRNA and were treated with a single addition of 2 or 4 mM H₂O₂. Cell viability was measured after 24 h of incubation.

Quantitative image analysis

Images were analyzed from three independent biological samples in three experimental repetitions (laminules). Three to five images from each replicate were recorded by confocal laser scanning microscope (LSM 710, Zeiss). For image analysis, the average fluorescence intensity per cell area in mm² was calculated using the ZEN 2.3 software (blue edition, Carl Zeiss Microscopy GmbH, 2011), and cells and nuclei were counted using the Cell Counter plugin of ImageJ software. Percentage calculations as well as statistical and graphical analyses were performed using the GraphPad Prism v.6.0 software.

Statistical analysis

The experiments were performed in three independent biological samples with three experimental repetitions each, from which all values are expressed as mean \pm SD. The data were checked for normal distribution using the Shapiro-Wilk

test. When normality was confirmed, statistical significance was evaluated by unidirectional and bidirectional ANOVA to determine significant differences between groups. Tukey's test was used to compare data between groups. Significance was established and represented as follows: $p < 0.05$ (*), $p < 0.01$ (**), $p < 0.0001$ (***), for comparisons with control, and $p < 0.05$ (#), $p < 0.01$ (##), $p < 0.0001$ (###) for comparisons between two time points within the same treatment.

Data availability

All data are contained within the article.

Supporting information—This article contains supporting information.

Acknowledgments—The authors are grateful to Brazilian agencies for supporting this project. This study was funded in part by the Coordenação de Aperfeiçoamento de Pessoal de Nível Superior - Brazil (CAPES) - Finance Code 001, CNPq-Instituto Nacional de Ciência e Tecnologia de Entomologia Molecular and FAPERJ.

Author contributions—B. D. N., C. C., and R. M. d. S. formal analysis; B. D. N., C. C., R. M. d. S., A. A., and M. V. d. C. U. investigation; I. d. S. V. Jr, S. K., K. O., and C. L. resources; R. M. d. S., I. d. S. V. Jr, S. K., and K. O. writing – original draft; L. A. d. A. and S. S. d. C. writing – review & editing; C. L. supervision; C. L. project administration.

Conflict of interest—The authors declare that they have no conflicts of interest with the contents of this article.

Abbreviations—The abbreviations used are: ETS, electron transport system; G6P, glucose 6-phosphate; G6PDH, glucose-6-phosphate dehydrogenase; GDE, glycogen debranching enzyme; GS, glycogen synthase; GSK3 β , glycogen synthase kinase 3 β ; HK, hexokinase; ICDH, isocitrate dehydrogenase; IGF, insulin-like growth factor; ISP, insulin-signaling pathway; LDH, lactate dehydrogenase; OCR, oxygen consumption rate; PEPCK, phosphoenolpyruvate carbox-kinase; PK, pyruvate kinase; ROS, reactive oxygen species.

References

1. Vleck, C., and Hoyt, D. (1991) Metabolism and energetic of reptilian and avian embryos. In *Egg Incubation: Its Effects on Embryonic Development in Birds and Reptiles*, Cambridge Univ. Press, Cambridge, UK: 285–306
2. Thompson, M. B., and Stewart, J. R. (1997) Embryonic metabolism and growth in lizards of the genus eumeces. *Comp. Biochem. Physiol. A Physiol.* **118**, 647–654
3. Yamamoto, Y., and Takahashi, S. Y. (1993) Cysteine proteinase from Bombyx eggs: Role in programmed degradation of yolk proteins during embryogenesis. *Comp. Biochem. Physiol. B* **106**, 35–45
4. Logullo, C., Da Silva Vaz, I., Sorgine, M. H. F., Paiva-Silva, G. O., Faria, F. S., Zingali, R. B., De Lima, M. F. R., Abreu, L., Fialho Oliveira, E., Alves, E. W., Masuda, H., Gonzales, J. C., Masuda, A., and Oliveira, P. L. (1998) Isolation of an aspartic proteinase precursor from the egg of a hard tick, *Boophilus microplus*. *Parasitology* **116**, 525–532
5. Fagotto, F. (1990) Yolk degradation in tick eggs: I. Occurrence of a cathepsin L-like acid proteinase in yolk spheres. *Arch. Insect Biochem. Physiol.* **14**, 217–235
6. Reiter, L. T., Potocki, L., Chien, S., Gribskov, M., and Bier, E. (2001) A systematic analysis of human disease-associated gene sequences in *Drosophila melanogaster*. *Genome Res.* **11**, 1114–1125

7. Herranz, H., and Cohen, S. M. (2017) *Drosophila* as a model to study the link between metabolism and cancer. *J. Dev. Biol.* **5**, 15
8. Gonzalez, C. (2013) *Drosophila melanogaster*: A model and a tool to investigate malignancy and identify new therapeutics. *Nat. Rev. Cancer* **13**, 172–183
9. [preprint] Devilliers, M., Garrido, D., Poidevin, M., Rubin, T., Le Rouzic, A., and Montagne, J. (2019) Differential metabolic sensitivity of insulin-like-response- and mTORC1-dependent overgrowth in *Drosophila* fat cells. *bioRxiv*. <https://doi.org/10.1101/606699>
10. Das, R., Sebo, Z., Pence, L., and Dobens, L. L. (2015) Erratum: *Drosophila* tribbles antagonizes insulin signaling-mediated growth and metabolism via interactions with Akt kinase. *PLoS One* **9**, e109530
11. Ren, S., Huang, Z., Jiang, Y., and Wang, T. (2018) dTBC1D7 regulates systemic growth independently of TSC through insulin signaling. *J. Cell Biol.* **217**, 517–526
12. Hietakangas, V., and Cohen, S. M. (2009) Regulation of tissue growth through nutrient sensing. *Annu. Rev. Genet.* **43**, 389–410
13. Oldham, S., and Hafen, E. (2003) Insulin/IGF and target of rapamycin signaling: A tor de force in growth control. *Trends Cell Biol.* **13**, 79–85
14. Teleman, A. A. (2010) Molecular mechanisms of metabolic regulation by insulin in *Drosophila*. *Biochem. J.* **425**, 13–26
15. de Abreu, L. A., Fabres, A., Esteves, E., Masuda, A., da Silva Vaz, I., Daffre, S., and Logullo, C. (2009) Exogenous insulin stimulates glycogen accumulation in *Rhipicephalus* (*Boophilus*) microplus embryo cell line BME26 via PI3K/AKT pathway. *Comp. Biochem. Physiol. B Biochem. Mol. Biol.* **153**, 185–190
16. de Abreu, L. A., Calixto, C., Waltero, C. F., Della Noce, B. P., Githaka, N. W., Seixas, A., Parizi, L. F., Konnai, S., Vaz, I. da S. J., Ohashi, K., and Logullo, C. (2013) The conserved role of the AKT/GSK3 axis in cell survival and glycogen metabolism in *Rhipicephalus* (*Boophilus*) microplus embryo tick cell line BME26. *Biochim. Biophys. Acta* **1830**, 2574–2582
17. Pavlova, N. N., and Thompson, C. B. (2016) The emerging hallmarks of cancer metabolism. *Cell Metab.* **23**, 27–47
18. Brand, K., Leibold, W., Lupp, P., Schoerner, C., and Schulz, A. (1986) Metabolic alterations associated with proliferation of mitogen-activated lymphocytes and of lymphoblastoid cell lines: Evaluation of glucose and glutamine metabolism. *Immunobiology* **173**, 23–34
19. Chambers, J. W., Maguire, T. G., and Alwine, J. C. (2010) Glutamine metabolism is essential for human cytomegalovirus infection. *J. Virol.* **84**, 1867–1873
20. Noch, E., and Khalili, K. (2012) Oncogenic viruses and tumor glucose metabolism: Like kids in a candy store. *Mol. Cancer Ther.* **11**, 14–23
21. Hay, N. (2016) Reprogramming glucose metabolism in cancer: Can it be exploited for cancer therapy? *Nat. Rev. Cancer* **16**, 635–649
22. De Berardinis, R. J., and Chandel, N. S. (2016) Fundamentals of cancer metabolism. *Sci. Adv.* **2**, e1600200
23. Carvalho-Santos, Z., Cardoso-Figueiredo, R., Elias, A. P., Tastekin, I., Baltazar, C., and Ribeiro, C. (2020) Cellular metabolic reprogramming controls sugar appetite in *Drosophila*. *Nat. Metab.* **2**, 958–973
24. Cully, M., You, H., Levine, A. J., and Mak, T. W. (2006) Beyond PTEN mutations: The PI3K pathway as an integrator of multiple inputs during tumorigenesis. *Nat. Rev. Cancer* **6**, 184–192
25. Sever, R., and Brugge, J. S. (2015) Signal transduction in cancer. *Cold Spring Harb. Perspect. Med.* **5**, a006098
26. Takahashi, N., Chen, H. Y., Harris, I. S., Stover, D. G., Selfors, L. M., Bronson, R. T., Deraedt, T., Cichowski, K., Welm, A. L., Mori, Y., Mills, G. B., and Brugge, J. S. (2018) Cancer cells co-opt the neuronal redox-sensing channel TRPA1 to promote oxidative-stress tolerance. *Cancer Cell* **33**, 985–1003.e7
27. Gorrini, C., Harris, I. S., and Mak, T. W. (2013) Modulation of oxidative stress as an anticancer strategy. *Nat. Rev. Drug Discov.* **12**, 931–947
28. Perillo, B., Di Donato, M., Pezone, A., Di Zazzo, E., Giovannelli, P., Galasso, G., Castoria, G., and Migliaccio, A. (2020) ROS in cancer therapy: The bright side of the moon. *Exp. Mol. Med.* **52**, 192–203
29. Gutzeit, H. O., Zissler, D., Grau, V., Liphardt, M., and Heinrich, U. R. (1994) Glycogen stores in mature ovarian follicles and young embryos of *Drosophila*: Ultrastructural changes and some biochemical correlates. *Eur. J. Cell Biol.* **63**, 52–60
30. Gutzeit, H. O., Zissler, D., and Fleig, R. (1993) Oogenesis in the honeybee *Apis mellifera*: Cytological observations on the formation and differentiation of previtellogenic ovarian follicles. *Roux Arch. Dev. Biol.* **202**, 181–191
31. Della Noce, B., de Carvalho Uhl, M. V., Machado, J., Waltero, C. F., de Abreu, L. A., da Silva, R. M., da Fonseca, R. N., de Barros, C. M., Sabadin, G., Konnai, S., da Silva Vaz, I., Ohashi, K., and Logullo, C. (2019) Carbohydrate metabolic compensation coupled to high tolerance to oxidative stress in ticks. *Sci. Rep.* **9**, 1–16
32. Esteves, E., Lara, F. A., Lorenzini, D. M., Costa, G. H. N., Fukuzawa, A. H., Pressinotti, L. N., Silva, J. R. M. C., Ferro, J. A., Kurtti, T. J., Munderloh, U. G., and Daffre, S. (2008) Cellular and molecular characterization of an embryonic cell line (BME26) from the tick *Rhipicephalus* (*Boophilus*) microplus. *Insect Biochem. Mol. Biol.* **38**, 568–580
33. Marinho, H. S., Cyrne, L., Cadenas, E., and Antunes, F. (2013) H2O2 delivery to cells: Steady-state versus bolus addition. *Methods Enzymol.* **526**, 159–173
34. Warburg, O. (1924) Über den Stoffwechsel der Carcinomzelle. *Naturwissenschaften* **12**, 1131–1137
35. Warburg, O. (1956) On the origin of cancer cells. *Science* **123**, 309–314
36. Warburg, O., Wind, F., and Negelein, E. (1927) The metabolism of tumors in the body. *J. Gen. Physiol.* **8**, 519–530
37. Hanahan, D., and Weinberg, R. A. (2011) Hallmarks of cancer: The next generation. *Cell* **144**, 646–674
38. Liberti, M. V., and Locasale, J. W. (2016) The warburg effect: How does it benefit cancer cells? *Trends Biochem. Sci.* **41**, 211–218
39. Furuta, E., Okuda, H., Kobayashi, A., and Watabe, K. (2010) Metabolic genes in cancer: Their roles in tumor progression and clinical implications. *Biochim. Biophys. Acta Rev. Cancer* **1805**, 141–152
40. da Silva, R. M., Della Noce, B., Fernanda Waltero, C., Costa, E. P., de Abreu, L. A., Githaka, N. W., Moraes, J., Gomes, H. F., Konnai, S., da Silva Vaz, I., Ohashi, K., and Logullo, C. (2015) Non-classical gluconeogenesis-dependent glucose metabolism in *Rhipicephalus* microplus embryonic cell line BME26. *Int. J. Mol. Sci.* **16**, 1821–1839
41. Fabres, A., De Andrade, C. P., Guizzo, M., Sorgine, M. H. F., Paiva-Silva, G. de O., Masuda, A., Da Silva vaz, I., and Logullo, C. (2010) Effect of GSK-3 activity, enzymatic inhibition and gene silencing by RNAi on tick oviposition and egg hatching. *Parasitology* **137**, 1537–1546
42. Logullo, C., Witola, W. H., Andrade, C., Abreu, L., Gomes, J., da Silva Vaz, I., Imamura, S., Konnai, S., Ohashi, K., and Onuma, M. (2009) Expression and activity of glycogen synthase kinase during vitellogenesis and embryogenesis of *Rhipicephalus* (*Boophilus*) microplus. *Vet. Parasitol.* **161**, 261–269
43. Moraes, J., Galina, A., Alvarenga, P. H., Rezende, G. L., Masuda, A., da Silva Vaz, I., and Logullo, C. (2007) Glucose metabolism during embryogenesis of the hard tick *boophilus* microplus. *Comp. Biochem. Physiol. A Mol. Integr. Physiol.* **146**, 528–533
44. Heiden, M. G. V., Cantley, L. C., and Thompson, C. B. (2009) Understanding the Warburg effect: The metabolic requirements of cell proliferation. *Science* **324**, 1029–1033
45. Exton, J. H., and Park, C. R. (1967) Control of gluconeogenesis in liver. I. General features of gluconeogenesis in the perfused livers of rats. *J. Biol. Chem.* **242**, 2622–2636
46. Yang, J., Reshef, L., Cassuto, H., Aleman, G., and Hanson, R. W. (2009) Aspects of the control of phosphoenolpyruvate carboxykinase gene transcription. *J. Biol. Chem.* **284**, 27031–27035
47. Hanson, R. W., and Reshef, L. (2003) Glyceroneogenesis revisited. *Biochimie* **85**, 1199–1205
48. Cantley, L. C. (2002) The phosphoinositide 3-kinase pathway. *Science* **296**, 1655–1657
49. Le Roith, D., and Zick, Y. (2001) Recent advances in our understanding of insulin action and insulin resistance. *Diabetes Care* **24**, 588–597
50. Shekar, S. C., Wu, H., Fu, Z., Yip, S. C., Nagajyothi, Cahill, S. M., Girvin, M. E., and Backer, J. M. (2005) Mechanism of constitutive phosphoinositide 3-kinase activation by oncogenic mutants of the p85 regulatory subunit. *J. Biol. Chem.* **280**, 27850–27855
51. Molinaro, A., Becattini, B., and Solinas, G. (2020) Insulin signaling and glucose metabolism in different hepatoma cell lines deviate from

Redox imbalance remodels the tick glucose metabolism

- hepatocyte physiology toward a convergent aberrant phenotype. *Sci. Rep.* **10**, 12031
52. Salvemini, D., and Cuzzocrea, S. (2002) Oxidative stress in septic shock and disseminated intravascular coagulation. *Free Radic. Biol. Med.* **33**, 1173–1185
 53. Halliwell, B. (1993) The role of oxygen radicals in human disease, with particular reference to the vascular system. *Pathophysiol. Haemost. Thromb.* **23**, 118–126
 54. Mittler, R. (2017) ROS are good. *Trends Plant Sci.* **22**, 11–19
 55. Finkel, T. (1998) Oxygen radicals and signaling. *Curr. Opin. Cell Biol.* **10**, 248–253
 56. Forman, H. J., Fukuto, J. M., and Torres, M. (2002) Redox signaling: Thiol chemistry defines which reactive oxygen and nitrogen species can act as second messengers. *Am. J. Physiol. Cell Physiol.* **287**, C246–C256
 57. Dröge, W. (2002) Free radicals in the physiological control of cell function. *Physiol. Rev.* **82**, 47–95
 58. Thannickal, V. J., and Fanburg, B. L. (2000) Reactive oxygen species in cell signaling. *Am. J. Physiol. Lung Cell. Mol. Physiol.* **279**, L1005–28
 59. Lambers, H., Szaniawski, R. K., and de Visser, R. (1983) Respiration for growth, maintenance and ion uptake. An evaluation of concepts, methods, values and their significance. *Physiol. Plant* **58**, 556–563
 60. Rzezniczak, T. Z., and Merritt, T. J. S. (2012) Interactions of NADP-reducing enzymes across varying environmental conditions: A model of biological complexity. *G3 (Bethesda)* **2**, 1613–1623
 61. King, I., Tsai, L. T. Y., Pflanz, R., Voigt, A., Lee, S., Jäckle, H., Lu, B., and Heberlein, U. (2011) *Drosophila* tao controls mushroom body development and ethanol-stimulated behavior through par-1. *J. Neurosci.* **31**, 1139–1148
 62. Monge-Fuentes, V., Gomes, F. M. M., Campos, G. A. A., Silva, J. de C., Biolchi, A. M., dos Anjos, L. C., Gonçalves, J. C., Lopes, K. S., and Mortari, M. R. (2015) Neuroactive compounds obtained from arthropod venoms as new therapeutic platforms for the treatment of neurological disorders. *J. Venom. Anim. Toxins Incl. Trop. Dis.* **21**, 31
 63. Pakpour, N., Camp, L., Smithers, H. M., Wang, B., Tu, Z., Nadler, S. A., and Luckhart, S. (2013) Protein kinase C-dependent signaling controls the midgut epithelial barrier to malaria parasite infection in anopheline mosquitoes. *PLoS One* **8**, e76535
 64. Bottino-Rojas, V., Talyuli, O. A. C., Jupatanakul, N., Sim, S., Dimopoulos, G., Venancio, T. M., Bahia, A. C., Sorgine, M. H., Oliveira, P. L., and Paiva-Silva, G. O. (2015) Heme signaling impacts global gene expression, immunity and dengue virus infectivity in *Aedes aegypti*. *PLoS One* **10**, e0135985
 65. Esteves, E., Bastos, C. V., Zivkovic, Z., de La Fuente, J., Kocan, K., Blouin, E., Ribeiro, M. F. B., Passos, L. M. F., and Daffre, S. (2009) Propagation of a Brazilian isolate of *Anaplasma marginale* with appendage in a tick cell line (BME26) derived from *Rhipicephalus (Boophilus) microplus*. *Vet. Parasitol.* **161**, 150–153
 66. Hambarde, S., Singh, V., and Chandna, S. (2013) Evidence for involvement of cytosolic thioredoxin peroxidase in the excessive resistance of Sf9 Lepidopteran insect cells against radiation-induced apoptosis. *PLoS One* **8**, 58261
 67. Pohl, P. C., Carvalho, D. D., Daffre, S., da Silva Vaz, I., and Masuda, A. (2014) *In vitro* establishment of ivermectin-resistant *Rhipicephalus microplus* cell line and the contribution of ABC transporters on the resistance mechanism. *Vet. Parasitol.* **204**, 316–322
 68. Kumar, J. S., Suman, S., Singh, V., and Chandna, S. (2012) Radioresistant Sf9 insect cells display moderate resistance against cumene hydroperoxide. *Mol. Cell. Biochem.* **367**, 141–151
 69. Cadena-Herrera, D., Esparza-De Lara, J. E., Ramírez-Ibañez, N. D., López-Morales, C. A., Pérez, N. O., Flores-Ortiz, L. F., and Medina-Rivero, E. (2015) Validation of three viable-cell counting methods: Manual, semi-automated, and automated. *Biotechnol. Rep.* **7**, 9–16
 70. Schindelin, J., Arganda-Carreras, I., Frise, E., Kaynig, V., Longair, M., Pietzsch, T., Preibisch, S., Rueden, C., Saalfeld, S., Schmid, B., Tinevez, J. Y., White, D. J., Hartenstein, V., Eliceiri, K., Tomancak, P., et al. (2012) Fiji: An open-source platform for biological-image analysis. *Nat. Methods* **9**, 676–682
 71. Zou, C., Wang, Y., and Shen, Z. (2005) 2-NBDG as a fluorescent indicator for direct glucose uptake measurement. *J. Biochem. Biophys. Methods* **64**, 207–215
 72. Smith, P. K., Krohn, R. I., Hermanson, G. T., Mallia, A. K., Gartner, F. H., Provenzano, M. D., Fujimoto, E. K., Goeke, N. M., Olson, B. J., and Klenk, D. C. (1985) Measurement of protein using bicinchoninic acid. *Anal. Biochem.* **150**, 76–85
 73. Pfaffl, M. W. (2001) A new mathematical model for relative quantification in real-time RT-PCR. *Nucleic Acids Res.* **29**, e45
 74. Nijhof, A., Balk, J. A., Postigo, M., and Jongejan, F. (2009) Selection of reference genes for quantitative RT-PCR studies in *Rhipicephalus (Boophilus) microplus* and *Rhipicephalus appendiculatus* ticks and determination of the expression profile of Bm86. *BMC Mol. Biol.* **10**, 112